Effects of Hydrogen Bonds on the Redox Potential and Electronic Structure of the Bacterial Primary Electron Donor†

Anabella Ivancich,‡ Katie Artz,§ JoAnn C. Williams,§ James P. Allen,§ and Tony A. Mattioli*,‡,||

Section de Biophysique des Protéines et des Membranes, Département de Biologie Cellulaire et Moléculaire, CEA and URA 2096, CEA Saclay, 91191 Gif-sur-Yvette Cedex, France, and Department of Chemistry and Biochemistry and Center for the Study of Early Events in Photosynthesis, Box 871604, Arizona State University, Tempe, Arizona 85287-1604

Received March 25, 1998; Revised Manuscript Received June 23, 1998

ABSTRACT: The primary donor, P, of photosynthetic bacterial reaction centers (RCs) is a dimer of excitonically interacting bacteriochlorophyll (BChl) molecules. The two constituents are named P_L and P_M to designate their close association with the L- and M-subunits, respectively, of the RC protein. A series of site-directed mutants of RCs from *Rhodobacter sphaeroides* has been constructed in order to model the effects of hydrogen bonding on the redox midpoint potential and electronic structure of P. The leucine residue at position M160 was genetically replaced with eight other amino acid residues capable of donating a hydrogen bond to the C_9 keto carbonyl group of the P_M BChl *a* molecule of P. Fourier transform (FT) (pre)resonance Raman spectroscopy with 1064 nm excitation was used to (i) determine the formation and strengths of hydrogen bonds on this latter keto carbonyl group in the reduced, neutral state (P^O), and (ii) determine the degree of localization of the positive charge on one of the two constituent BChl molecules of P in its oxidized, radical cation state ($P^{\bullet+}$). A correlation was observed between the strength of the hydrogen bond and the increase in $P^O/P^{\bullet+}$ redox midpoint potential. This correlation is less pronounced than that observed for another series of RC mutants where hydrogen bonds to the four π-conjugated carbonyl groups of P were broken or formed uniquely involving histidinyl residues [Mattioli, T. A., Lin, X., Allen, J. P. and Williams, J. C. (1995) *Biochemistry 34*, 6142−6152], indicating that histidinyl residues are more effective in raising the $P^O/P^{\bullet+}$ redox midpoint potential via hydrogen bond formation than are other hydrogen bond-forming residues. In addition, an increase in positive charge localization is correlated with the strength of the hydrogen bond and with the $P^O/P^{\bullet+}$ redox midpoint potential. This latter correlation was analyzed using an asymmetric bacteriochlorophyll dimer model based on Hückel-type molecular orbitals in order to obtain estimates of certain energetic parameters of the primary donor. Based on this model, the correlation is extrapolated to the case of complete localization of the positive charge on P_L and gives a predicted value for the P/P^+ redox midpoint potential similar to that experimentally determined for the *Rb. sphaeroides* HL(M202) heterodimer. The model yields parameters for the highest occupied molecular orbital energies of the two BChl *a* constituents of P which are typical for the oxidation potential of isolated BChl *a* in vitro, suggesting that the protein, as compared to many solvents, does not impart atypical redox properties to the BChl *a* constituents of P.

The photosynthetic reaction center (RC)[1] of purple photosynthetic bacteria is an integral membrane protein wherein the primary light reactions resulting in stable transmembrane charge separation occur (for reviews, see ref *1*−*3*). The three-dimensional structures of RCs from two species of purple bacteria, *Rhodopseudomonas* (*Rps.*) *viridis* and *Rhodobacter* (*Rb.*) *sphaeroides*, have been elucidated by X-ray diffraction (*4*−*10*). The RC photochemistry is initiated by the photoexcitation of the primary electron donor (P) which is a dimer of excitonically interacting bacteriochlorophyll (BChl) molecules, whose constituents are named P_L and P_M reflecting their association with the L and M protein subunits of the RC. The physicochemical properties and electronic structure of the primary donor are critical for the efficient functioning of the RC (for review, see ref *11*).

The primary donor is a crucial redox component in the RC and thus its oxidation potential is expected to be an important property in all the electron transfer reactions involving P. The physicochemical properties of the two BChl molecules of P are largely defined by the extensive π-electronic system of their macrocycles. Each BChl molecule of P possesses two π-conjugated carbonyl groups, the C_2 acetyl and the C_9 keto carbonyl. It has been shown

† A.I. acknowledges a postdoctoral fellowship from CONICET (Argentina). Financial support from the U.S. Department of Agriculture (97-35303-4524) is acknowledged.

* Corresponding author.

‡ CEA and URA 2096, CEA Saclay.

§ Arizona State University.

|| Present address: IDS, Intelligent Detection Systems, 152 Cleopatra Dr., Nepean, Ontario K2G5X2, Canada. Email: tmattioli@idsdetection.com. Fax: (613) 224 2603.

[1] Abbreviations: BChl, bacteriochlorophyll; EDTA, ethylenediaminetetraacetic acid; ENDOR, electron nuclear double resonance; HOMO, highest occupied molecular orbital; LDAO, lauryl dimethylamine oxide; LUMO, lowest unoccupied molecular orbital; P, primary electron donor; *Rb.*, *Rhodobacter*; RC, reaction center; *Rps. Rhodopseudomonas*; Tris, tris(hydroxymethyl)aminomethane.

S0006-2960(98)00690-4 CCC: $15.00
Published on Web 08/01/1998

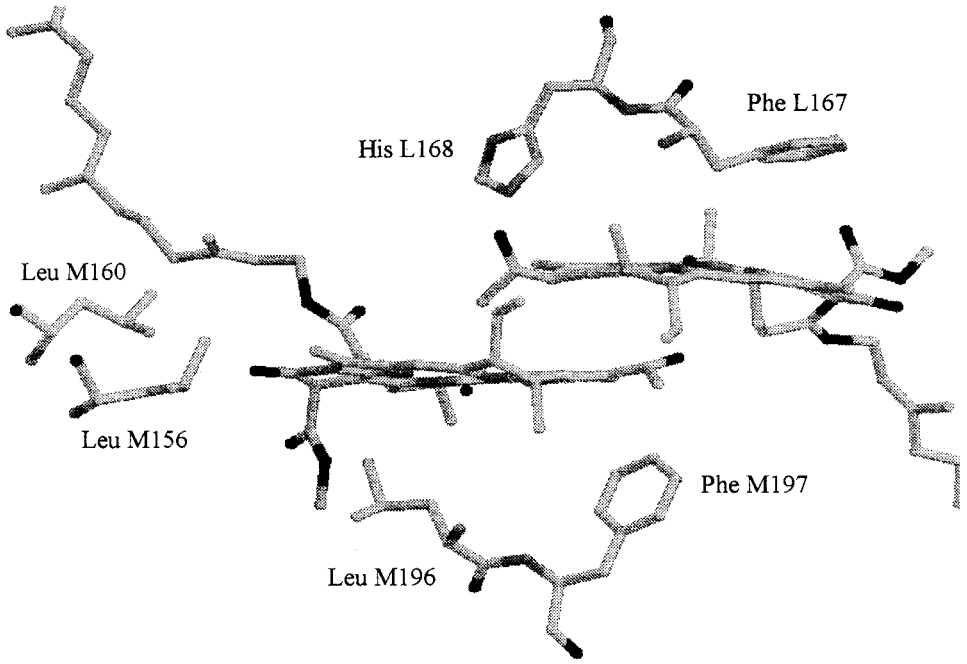

FIGURE 1: The two bacteriochlorophyll *a* molecules (P_L and P_M) of the primary donor of *Rb. sphaeroides*. The axial ligands are not shown. Leucine M160 is in close proximity to the C_9 keto carbonyl of P_M. Also shown are the residues His L168, which is engaged in a H-bond with the C_2 acetyl carbonyl of P_L, Phe M197, Phe L167, Leu M196, and Leu M156.

that the addition of H-bonds, donated by histidinyl residues, to the conjugated carbonyl groups of the primary donor in *Rb. sphaeroides* RCs systemmatically raises its $P^O/P^{\bullet+}$ redox midpoint potential from 410 mV (for the case of no H-bonds) to 765 mV (for the case of four H-bonds) (*12*, *13*). The increase in the P midpoint potential was observed to correlate with the strength of the H-bonds on the π-conjugated C_2 acetyl and C_9 keto carbonyl groups (*14*), and a linear relationship was found between the $P^O/P^{\bullet+}$ redox midpoint potential and the cumulative strengths of multiple histidine-donated H-bonds to P (*13*). However, comparison of two similar mutants of *Rb. sphaeroides*, one where phenylalanine M197 was genetically replaced by histidine (*14*) and one where it was replaced by tyrosine (*15*), revealed that a tyrosine-donated H-bond to the C_2 acetyl carbonyl group of P_M only modestly raised the $P^O/P^{\bullet+}$ redox midpoint potential by 25 mV while the histidine-donated H-bond, of comparable strength, to the same carbonyl group raised this potential by 125 mV. This significant difference in the raising of the midpoint potential suggested that the chemical nature of the amino acid donating the H-bond to P may be a significant factor in this mechanism (*13*).

In this paper, we report the effects of H-bonding to P with amino acid residues other than histidine and assess to what extent H-bonds can influence the $P^O/P^{\bullet+}$ redox midpoint potential. The target site was leucine M160 in the reaction center of *Rb. sphaeroides* (see Figure 1), and it has been genetically replaced with lysine, serine, asparagine, aspartic acid, glutamine, glutamic acid, and tyrosine as well as histidine. Leu M160 is in close proximity to the C_9 keto carbonyl group of P_M, and the replacement of Leu M160 with His has been shown to result in the formation of a H-bond with this carbonyl group (*14*, *16*). In this work, Fourier transform (FT) Raman spectroscopy was used to determine the hydrogen bonding state of the P_M C_9 keto carbonyl group in mutant reaction centers bearing the above-mentioned residues at position M160, and to estimate the H-bond enthalpy which was correlated with the previously reported change in the $P^O/P^{\bullet+}$ redox midpoint potential (*17*). Furthermore, this change in the $P^O/P^{\bullet+}$ redox midpoint potential was related to the degree of positive charge localization on P_L in the $P^{\bullet+}$ oxidized radical cation using a simple Hückel molecular orbital model of an asymmetric dimer originally described by Plato (*18*) and by Parson (*19*, *20*) and their co-workers. These changes due to mutations at Leu M160 are compared to the effects of mutations of other residues near P, including Phe L167, Leu M156, and Leu M196.

MATERIALS AND METHODS

Mutagenesis, Bacterial Growth and Reaction Center Isolation. Rb. sphaeroides reaction center mutants were constructed by oligonucleotide-directed mutagenesis as described previously (*17*, *21*−*23*). The genes were expressed in the *Rb. sphaeroides* deletion strain ΔLM1.1 (*24*). The term "wild type (WT) RCs" described in this paper refers to those isolated from the deletion strain complemented with a plasmid bearing the wild-type RC genes. The *Rb. sphaeroides* mutants were grown under nonphotosynthetic conditions, and the RCs were isolated using procedures described previously (*21*). Final RC proteins were in 15 mM Tris-HCl, pH 8, 0.025% LDAO, and 1 mM EDTA.

Redox Titrations and Fourier Transform Raman Spectroscopy. Redox titrations on isolated reaction centers were performed as previously described (*21*, *22*). Room-temperature Fourier transform Raman spectra were recorded using a Bruker IFS 66 interferometer coupled to a Bruker FRA 106 Raman module and is described elsewhere (*25*). Typically, no more than 180 mW of laser power was used, and the spectral resolution was 4 cm^{-1}. RC samples were in 15 mM Tris-HCl, pH 8, 0.025% LDAO, 1 mM EDTA and were concentrated to ca. 150 OD at 800 nm using a Centricon microconcentrating system (Amicon). Samples were poised

Table 1: Observed Vibrational Frequencies of the C_9 Keto Carbonyl Groups, Calculated H-Bond Enthalpies, Determined Localization of Positive Charge over $P^{\bullet+}$, and Changes in $P^{o}/P^{\bullet+}$ Midpoint Potential for the M160 Series of RC Mutants from *Rb. sphaeroides*

mutant	residue at M160	P_M C_9=O (cm^{-1})	$\Delta\nu$[a] (cm^{-1})	ΔH[b] (meV)	P_L C_9=O (P^o)[c] (cm^{-1})	P_L C_9=O ($P^{\bullet+}$)[d] (cm^{-1})	% local. on P_L[e]	ρ_L from ENDOR[f]	E_m (mV)[g]	ΔE_m (mV)[h]
WT	Leu	1679	–	–	1691.7	1715.0	72.8	68	506	–
LK(M160)	Lys	1679	0	0	1691.7	1715.5	74.4	66	511	5
LS(M160)	Ser	1664	15	94	1693.6	1715.3	67.8	68	514	8
LN(M160)	Asn	1665	14	88	1693.6	1716.3	70.9	70	527	21
LD(M160)	Asp	1656	23	145	1693.6	1716.7	72.2	74	539	33
LQ(M160)	Gln	1656	23	145	1694.0	1718.0	75.0	79	544	38
LE(M160)	Glu	1656	23	145	1694.2	1718.0	76.3	79	546	40
LY(M160)	Tyr	1656	23	145	1693.6	1718.7	78.4	82	558	52
LH(M160)	His	1656	23	145	1693.6	1718.7	78.4	83	563	57

[a] Difference in vibrational frequency of the P_M C_9 keto carbonyl with respect to WT. [b] Calculated H-bond enthalpy as described in ref *13*. [c] Vibrational frequency of the P_L C_9 keto carbonyl in the neutral P^o state. [d] Vibrational frequency of the P_L C_9 keto carbonyl in the oxidized $P^{\bullet+}$ state. [e] Percent localization of the positive charge on $P^{\bullet+}$ calculated from the oxidation-induced upshift of the P_L C_9 keto carbonyl vibrational frequency (*13, 25, 29*). [f] Unpaired electron spin density on P_L in the $P^{\bullet+}$ state as obtained from ENDOR measurements (*17*); expressed in the table in percent. [g] $P^o/P^{\bullet+}$ midpoint potential (*17*). [h] Difference in $P^o/P^{\bullet+}$ midpoint potential between mutant and wild type (*17*).

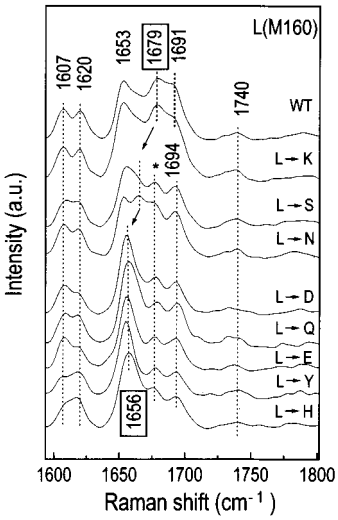

FIGURE 2: Fourier transform preresonance Raman spectra of several mutant RCs of *Rb. sphaeroides* bearing mutations at position M160. All RCs are in their neutral reduced P^o state. Room temperature, 4 cm^{-1} spectral resolution, coaddition of 4000 scans. The 1676 cm^{-1} band (*) in the LS, LN, LD, LQ, LE, LY, and LH(M160) spectra does not arise from P (see text).

in their reduced (P^o) and oxidized ($P^{\bullet+}$) states using sodium ascorbate and potassium ferricyanide, respectively. Reported frequencies are accurate to within ± 1 cm^{-1}. To improve the precision of the percent localization of the positive charge over $P^{\bullet+}$, the C_9 keto carbonyl stretching frequencies in Table 1 were obtained from second derivative analysis of the P and $P^{\bullet+}$ FT Raman spectra, and are reported to one decimal place. Spectral deconvolution and second derivative analyses were performed using GRAMS 32 (Galactic Industries).

RESULTS

Figure 2 shows the room-temperature P^o FT Raman spectra of WT and the *Rb. sphaeroides* M160 mutant RCs in the presence of ascorbate and excited with 1064 nm light. The assignments of the FT Raman bands corresponding to all four π-conjugated carbonyl group vibrators of P are discussed elsewhere (*13, 14, 25*). The C_9 keto carbonyl group of the P_M BChl constituent P is the conjugated carbonyl group closest to the Leu M160 residue (Figure 1); the Raman band corresponding to its vibrational stretching mode is observed at 1679 cm^{-1} in the WT P^o FT Raman spectrum (Figure 2). A mutation at position M160 which results in a H-bonding interaction with this keto carbonyl will cause its vibrational stretching mode frequency to decrease. The degree of this downshift in frequency reflects the strength of the interaction. This effect is readily seen in the P^o FT Raman spectra of all but one of the M160 RC mutants (Figure 2). For the cases of the LS(M160) and LN(M160) mutants, the 1679 cm^{-1} band is seen to downshift to 1664 cm^{-1}. For cases such as the LD, Q, E, Y, and H(M160) mutants, the 1679 cm^{-1} band downshifts to the same spectral region as the 1653 cm^{-1} band of the P_M C_2 acetyl carbonyl group, and so these two bands overlap. Both Fourier deconvolution and second-derivative analyses cannot separate the contributions of these two bands. In such cases, the frequency of the P_M C_9 keto carbonyl group is taken to be that of the resulting observed frequency of both bands. The error is estimated to be less than ± 5 cm^{-1}. Figure 2 clearly shows that the FT Raman spectrum of the LK(M160) mutant is very similar to that of WT and therefore this mutation does not result in the formation of a H-bond on the P_M C_9 keto carbonyl group.

The frequencies of the P_M C_9 keto carbonyl of all the M160 mutants are summarized in Table 1. The downshift of the 1679 cm^{-1} band exposes another band at 1676 cm^{-1} which was underneath this former band. The 1676 cm^{-1} band persists in the $P^{\bullet+}$ FT Raman spectrum and therefore cannot be assigned to any of the conjugated carbonyl groups of P^o. The 1676 cm^{-1} band has been discussed elsewhere (*13, 14*) as well as its possible origins (*26, 27*).

Figure 3 shows the $P^{\bullet+}$ FT Raman spectra of the M160 RC mutants. For the WT, when the primary donor is oxidized to its $P^{\bullet+}$ state, there is an oxidation-induced upshift of the 1691 cm^{-1} band, corresponding to the P_L C_9 keto carbonyl group in the P^o state, to 1715 cm^{-1} (*13, 14*). The magnitude of this 23−24 cm^{-1} upshift reflects the degree of localization of the resulting positive charge on the P_L constituent of dimeric P in its oxidized, radical cation state (*13, 14, 25, 28, 29*). In a simple model, we assume that the observed upshift in frequency of the P_L C_9 carbonyl stretching frequency is proportional to charge localization and that no other protein-induced BChl structural changes affecting this carbonyl frequency occur as a result of the oxidation (*25, 28*). Considering that a non-H-bonded keto carbonyl group of monomeric BChl $a^{\bullet+}$ (one-electron oxidation) in vitro upshifts +32 cm^{-1} (*30*−*33*), this upshift was taken to

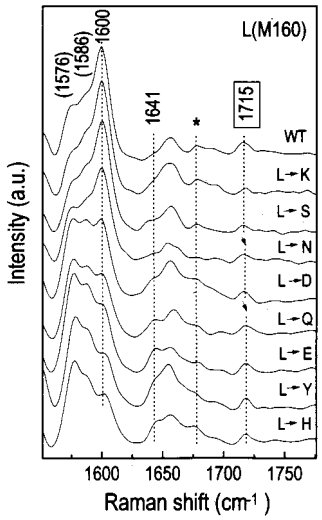

FIGURE 3: Fourier transform resonance Raman spectra of the M160 RC mutants in their oxidized $P^{\bullet+}$ state (RCs poised in ferricyanide). Same conditions as in Figure 2. The 1676 cm^{-1} band (*) in the LS, LN, LD, LQ, LE, LY, and LH(M160) spectra does not arise from P (see text).

represent 100% positive charge localization on one BChl molecule. Thus, the 23−24 cm^{-1} upshift observed for WT (*13*, *14*) corresponds in our model to 72−75% localization of the positive charge on P_L. The validity of the +32 cm^{-1} upshift has recently been tested in a mutant reaction center of *Rb. sphaeroides* in which the P_M constituent is a bacteriopheophytin molecule [the so-called heterodimer HL(M202) mutant] and where the positive charge resides wholly on the P_L BChl constituent (*29*).

Table 1 summarizes the percent localization of the positive charge on P_L for the M160 reaction center mutants as determined by FT Raman. For direct comparison, the unpaired electron spin density, ρ_L, estimated from the ENDOR measurements (*17*), has been converted to percent values. There is excellent agreement between these two different measurements.

Non-Hydrogen-Bonding Mutants. The $P^o/P^{\bullet+}$ redox potential may be altered without a change in the H-bond interactions of the π-conjugated carbonyl groups of P. Table 2 lists such changes in the midpoint potentials, observed for mutations at other residue positions that do not involve H-bonding to P. The largest changes in midpoint potential are observed for mutations that introduce a histidine while other substitutions result in increases of up to 30 mV (Table 2). None of these mutations change the H-bond interactions as measured by FT Raman spectroscopy (data not shown). Similar observations of the raising of the $P^o/P^{\bullet+}$ midpoint potential have been previously made with *Rb. sphaeroides* RCs bearing mutations at positions M210 (*34*) and L162 (*35*), residues which are not in direct H-bonding contact with the π-conjugated groups of P. The effects on the $P^o/P^{\bullet+}$ redox potential in other RC mutants which do not change the H-bonding states in P are summarized in Allen and Williams (*11*). Interestingly, the "non-H-bonding" mutations listed in Table 2 also affect the localization of the positive charge over $P^{\bullet+}$. The relationship between the localization and the midpoint potential is dependent upon the location of the altered amino acid residue. The substitution of Asn and His at M156 results in smaller absolute changes in the midpoint potential and localization compared to the same substitutions at M160; however, they all show a similar correlation between the midpoint potential and localization. Thus, the observed correlation between the localization and the P midpoint potential may not be restricted to amino acids in H-bonding position to the conjugated system.

DISCUSSION

In the M160 series of *Rb. sphaeroides* reaction center mutants reported here, we have studied the effects of different amino acid residues H-bonding to the C_9 keto carbonyl group of the P_M constituent of P, on the $P^o/P^{\bullet+}$ midpoint potential and the positive charge distribution over $P^{\bullet+}$. This work extends our knowledge of the specific role of H-bonding to the π-conjugated carbonyl groups of the bacterial primary donor pair in modulating its redox properties, and reveals the extent to which the P oxidation potential can be modified by typical protein H-bonds.

The strategy of choosing the single M160 position to study the effects of protein H-bonding to π-conjugated carbonyl groups of P may be summarized as follows:

1. Selecting one site instead of several sites near P reduces heterogeneous effects arising from slight environmental differences in each of the other sites near the four π-conjugated carbonyl groups of P.

2. The nearby π-conjugated carbonyl group of P is that of the C_9 keto carbonyl belonging to P_M. The keto carbonyl groups are not susceptible to significant changes in orientation with respect to the macrocycle of BChl; the C_2 acetyl carbonyl groups are susceptible to such orientational changes which are expected to appreciably alter the physicochemical properties of P (*36*) and, thus, its oxidation potential.

3. The region around position M160 is situated well within the transmembrane helical section of the RC, and is largely hydrophobic so that the presence and thus the effects of charged residues on the P midpoint potential should be minimized. One can expect the introduced residues, which may be potentially charged, to be in their neutral forms (e.g., protonated carboxylic acid residues which are capable of donating H-bonds). Furthermore, the C_2 acetyl carbonyl groups of P are located more to the outside of the transmembrane helices and thus are not in strictly hydrophobic environments. Amino acid residues in this region, which can H-bond to these acetyl carbonyl groups, may be involved in other H-bonds and may participate in H-bond networks (see, for example, ref *37*).

4. Genetically introduced amino acid residues at position M160 may form H-bonds on the C_9 keto carbonyl of P_M. By not perturbing the C_9 keto carbonyl of P_L, we may use its oxidation-induced upshift in frequency to accurately assess the positive localization over $P^{\bullet+}$ in the mutant RCs (see Results).

Figure 4 shows a plot of the $P^o/P^{\bullet+}$ redox midpoint potential and the strength of the H-bond formed on P for the M160 series of RC mutants. The estimated strengths of the H-bonds formed were calculated as described in ref *13* and are listed in Table 1. Within the sensitivity and resolution of our Raman measurements (see Results), a correlation between the strength of the H-bond to the P_M C_9 keto carbonyl and the $P^o/P^{\bullet+}$ redox midpoint potential can be seen, and can be considered linear, to a first approximation. A similar linear correlation was observed for a series

Table 2: Properties of *Rb. sphaeroides* RC Mutants with Mutations Near P but Not in H-Bonding Position

mutant	FL(L167)	FH(L167)	FY(L167)	LF(M196)	LH(M156)	LN(M156)
ΔE_m[a] (±5 mV)	+25	+37	+31	+13	+44	+2
% local. on P_L[b]	63	84	nd	72	75	65

[a] Change in the $P^o/P^{\bullet+}$ midpoint potential as compared to wild type. [b] Percent localization of the positive charge on $P^{\bullet+}$ calculated from the oxidation-induced upshift of the P_L C_9 keto carbonyl vibrational frequency (*13*, *25*, *29*).

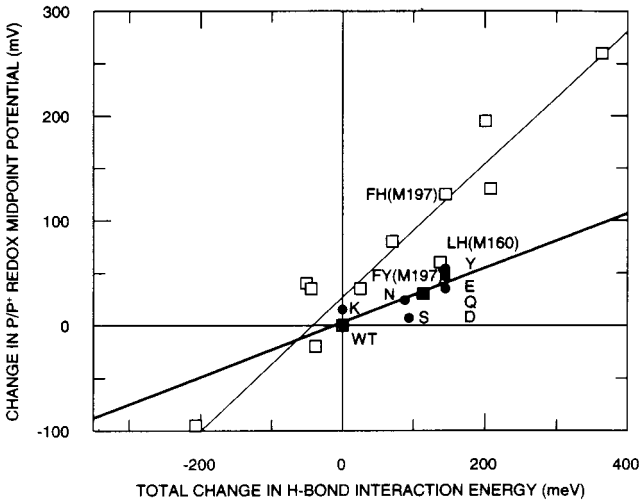

FIGURE 4: The change in the $P^o/P^{\bullet+}$ midpoint potentials for the M160 series of RC mutants of *Rb. sphaeroides* plotted as a function of the estimated H-bond energy (as described in ref *13*) on the P_M C_9 keto carbonyl of P (●); these data points are labeled using the one-letter code for the residue at position M160. Linear regression analysis of these points yields a line (thick line) of slope 0.259 mV/meV, an intercept of 3 mV, and a correlation coefficient of 0.819. Also shown are data from another series of *Rb. sphaeroides* RC mutants where H-bonds donated from histidinyl residues to all four conjugated carbonyl groups were formed or broken (□) (*13*), including the LH(M160) (*13*, *14*) as well as the FY(M197) RC mutant where a H-bond to the P_L C_2 acetyl carbonyl was formed with tyrosine residue (■) (*15*). This line (thin line) was fit with slope of 0.59 mV/meV, an intercept of 32 mV, and a correlation coefficient of 0.954 (*13*).

of *Rb. sphaeroides* RC mutants where H-bonds were formed on the four conjugated carbonyl groups of P via the introduction of (multiple) histidine residues (Figure 6 in ref *13*); however, the slope of the line describing that correlation was steeper in the latter work than it is for the M160 series reported here. Both correlations are presented in Figure 4 for direct comparison.

Figure 4 indicates that there are at least two types of lines which can describe the general correlation between the $P^o/P^{\bullet+}$ redox midpoint potential and H-bonding. The greater slope of the histidine series of mutants indicates that histidine residues, as H-bond donors to P, are more effective in raising its midpoint potential than are other H-bond donors of similar H-bonding strength. Consistent with this idea is the observation that, in the M160 series of mutants, the histidine mutation results in the greatest increase in the $P^o/P^{\bullet+}$ redox midpoint potential with a H-bond strength which is comparable to that of Tyr, Glu, Gln, and Asp (Table 1). The line describing the M160 series of RC mutants can be considered as reflecting the effects of H-bonding on the P redox potential without any additional effects which histidine residues may impart to the $P^o/P^{\bullet+}$ midpoint potential (see below).

The formation or rupture of H-bonds made by histidine residues to the conjugated carbonyl groups of P results in relatively large changes in its midpoint potential. The P_L C_2 acetyl carbonyl group of the WT *Rb. sphaeroides* primary donor is engaged in a H-bond with His L168 which when genetically removed results in a change of −95 mV in the $P^o/P^{\bullet+}$ redox midpoint potential. As was previously discussed, the relatively modest rise of 25 mV in the $P^o/P^{\bullet+}$ redox midpoint potential of the FY(M197) *Rb. sphaeroides* mutant, compared to that of 125 mV for the FH(M197) mutant in which a histidine forms a H-bond of comparable strength to the P_M C_2 acetyl carbonyl, should originate from the chemical differences between these two different H-bond donors (*13*). Accordingly, our results show that the FY(M197) data point falls onto the line describing the correlation for the M160 series of RC mutants.

From this work on the M160 series of RC mutants and that from previous work (*13*, *14*), we may note two important general observations: (i) it appears that histidine has the greatest effect in raising the midpoint potential of P when comparing other donors forming similar H-bonds of comparable strength (Figure 4); (ii) this effect appears to be greater for H-bonds to the C_2 acetyl carbonyls than for the C_9 keto carbonyls (see, for example, Table 1 in ref *13*). The reasons for these behaviors may be rationalized in terms of electrostatic and BChl conformational arguments:

(A) Electrostatic Effects. Histidine residues, in addition to H-bonding, may raise the redox potential of P via other electrostatic effects in which partial positive charges are nearby P. Although it cannot be formally excluded, there is no experimental data to suggest that the histidine residues forming H-bonds to P in the RC mutants, or His L168 in wild type, are protonated and therefore positively ionized. However, the histidinyl imidazole ring side chain, in its neutral state, possesses a larger dipole moment than that of tyrosine[2] and the other residues genetically introduced in this work. Furthermore, the histidinyl imidazole ring is capable of adopting resonance structures (*38*), one of which can be stabilized by H-bonding and place residual positive charge near the primary donor. However, the presence of partial or full charges is expected to be less probable in hydrophobic regions such as those found near the C_9 keto carbonyl groups of P. Additionally, there are greater chances of H-bond networking in the regions near the C_2 acetyl carbonyls (*37*) which could result in H-bonding to the histidine residues already H-bonded to the acetyl carbonyls of P.

(B) BChl Conformational Effects. It is generally accepted that the conformation of the BChl macrocycle (*39*) and, in particular, the orientation of the C_2 acetyl carbonyl groups significantly modulate the physicochemical properties of the BChl molecule (*36*). It is possible, therefore, that the

[2] The reported experimental values of the dipole moments (μ) of imidazole and phenol (in the gas phase) are 3.80 and 1.22 D, respectively [*CRC Handbook of Physical Chemistry* (Lide, D. R., Ed.) CRC Press, Boca Raton].

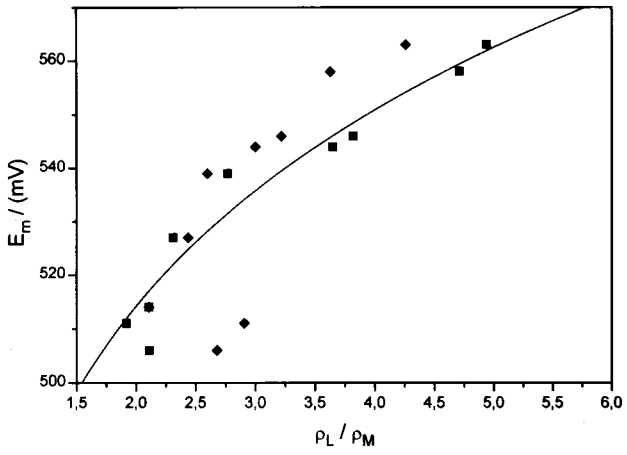

FIGURE 5: The $P^o/P^{\bullet+}$ midpoint potentials, E_m, for the M160 series of RC mutants of *Rb. sphaeroides* plotted as a function of the ratio of the unpaired electron spin densities of P_L and P, ρ_L/ρ_M. The spin densities (or percent localization of the positive charge) have been determined by FT Raman (◆) (see text) and ENDOR (■) data (*17*), and both sets of data are shown. The data were fit using eq 5 and gave values of $E_L = 680$ meV and $\beta_D = 240$ meV.

formation of H-bonds donated by histidine residues at positions L168 and M197 in *Rb. sphaeroides* RCs could result in orientations of the C_2 acetyl carbonyl groups of constituents P_L and P_M, respectively, which effectively raise the midpoint potential and could be significantly different for other H-bond-donating residues at the same positions. In the three-dimensional X-ray crystal structural model of the *Rb. sphaeroides* RC (*8*), the H-bonded C_2 acetyl carbonyl group of P_L makes an angle of ca. 90° with the macrocycle while that of P_M makes an angle of ca. 0° with the macrocycle. No such structure is available for the FH(M197) RC mutant.

H-Bonding and Localization of the Positive Charge in $P^{\bullet+}$. Table 1 indicates that there is a correlation between the $P^o/P^{\bullet+}$ redox midpoint and the degree of localization of the positive charge over $P^o/P^{\bullet+}$. A recent ENDOR study of these same M160 mutants has also revealed that the increase in $P^o/P^{\bullet+}$ redox midpoint potential is directly related to the amount of unpaired electron spin density on P_L (*17*). Figure 5 shows the experimental E_m primary donor midpoint potentials of the M160 mutants plotted as a function of $x = \rho_L/\rho_M$ (ratio of the unpaired electron spin density over P_L and P_M) as determined from the Raman data (Table 1) along with the ENDOR data (*17*) for comparison. Both the Raman data and the ENDOR data, plotted in Figure 5, show excellent quantitative agreement even though the models used to analyze the experimental data in terms of the positive charge localization or the unpaired electron spin density over $P^{\bullet+}$ in each case are qualitatively different.

Among several molecular orbital models developed to describe properties of the primary donor dimer (*18*−*20*, *40*−*42*), the effects of the H-bond on the $P^o/P^{\bullet+}$ redox midpoint potential have recently been examined by Artz et al. (*17*) and may be qualitatively understood in terms of a simple dimer Hückel-type molecular orbital (MO) model (*40*) of the primary donor, as proposed by Plato (*18*) and by Parson (*19*, *20*) and their co-workers. Figure 6 schematically shows the asymmetric dimer molecular orbital model of the primary electron donor of *Rb. sphaeroides* and depicts the energetic parameters discussed here. The individual P_L and P_M

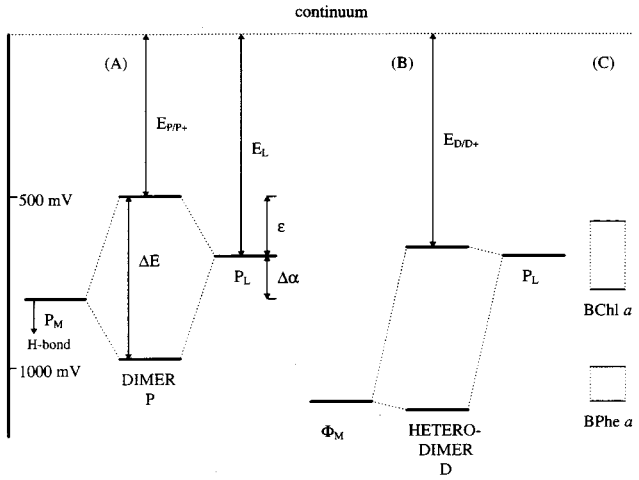

FIGURE 6: (A) Molecular orbital diagram of the model for the BChl *a* dimer of the reaction center from *Rb. sphaeroides*. Represented are the energy levels of the two highest occupied dimer molecular orbitals of P as well as of the HOMOs of P_L and P_M. For the M160 series of RC mutants, H-bonds to the C_9 keto carbonyl group of P_M are expected to stabilize its HOMO, thus resulting in a stabilization of the dimer HOMO and consequently a rise in the $P^o/P^{\bullet+}$ midpoint potential ($E_{P/P+}$) and localization of the positive charge (or unpaired spin density distribution) in $P^{\bullet+}$. Fitting the data in Figure 5 with eq 5 gives $E_L = 680$ meV and $\beta_D = 240$ meV (see Table 3 for the other values, $E_M = 800$ meV). (B) Extrapolation of the model in (A) for the case of the BChl−BPhe heterodimer. The energy of the HOMO of the BPhe constituent ($\Phi_M = 1100$ meV) used is that of the oxidation of BPhe *a* typically observed in vitro (see text for details). For the heterodimer, $E_L = 730$ meV (i.e., 50 meV higher than E_L in the WT homodimer) and $\beta_D = 190$ meV (i.e., 50 meV lower than β_D in the WT homodimer) give a $D^o/D^{\bullet+}$ midpoint potential of $E_{D/D+} = 650$ meV. (C) Ranges of typical oxidation potentials of BChl *a* and BPhe *a* in vitro.

monomer MOs are not isoenergetic, most likely due to any one, or a combination, of the following factors: (i) inequivalent protein environments and interactions; (ii) different orientation of substituent groups (e.g., C_2 acetyl carbonyls); or (iii) different conformations of the BChl macrocycles themselves. Adding a H-bond to the P_M constituent should stabilize its MO energy, and therefore the dimer redox orbital will increase in P_L character. This increase in P_L character will be reflected by observing an increase in positive charge localization (or unpaired spin density) on P_L estimated from the FT Raman (or ENDOR) spectrum of $P^{\bullet+}$. The stronger the H-bond on P_M, the greater the stabilization of its MO and thus the greater the unpaired electron (or hole) localization on P_L. Furthermore, the stabilization of the P_M MO due to H-bonding will also result in the general stabilization of the dimer redox MO, thereby resulting in a rise in the $P^o/P^{\bullet+}$ redox midpoint potential.

In the model shown in Figure 6, the individual P_L and P_M highest occupied molecular orbitals (HOMOs) differ in energy by an amount $\Delta\alpha$, and the intermolecular coupling interaction between P_L and P_M can be expressed by the resonance integral β_D. The Hückel theory relates the energy splitting, ΔE, of the dimer HOMO and lowest unoccupied molecular orbital (LUMO) as

$$\Delta E = [(\Delta\alpha)^2 + (2\beta_D)^2]^{1/2} \quad (1)$$

The ratio of unpaired electron spin density, ρ, over the P_L and P_M constituents can be written

Table 3: Modelling of the Wild-Type Dimer MO Energies

	E_L[a] (meV)	β_D[a] (meV)	$E_{D/D+}$[b]	E_M[a] (meV)	$\Delta\alpha$[a] (meV)	ΔE[a] (meV)	E_m[c]	ρ_L/ρ_M[a]
fitted values	680	240	680 meV[d]	800	120	494	495 meV	2.56
estimated errors	± 40		±40 meV	±40	±40	±8	±22 meV	±0.8 meV
measured values			640−660 mV[e]	?	?	320[f]	506 mV[g]	2.68,[h] 2.12[g,i]

[a] Parameters for wild type as defined in eqs 1−5 and depicted in Figure 6 (see text for details). [b] $D^{o}/D^{\bullet+}$ midpoint potential for the M202 heterodimer *Rb. sphaeroides* RC mutant. [c] $P^{o}/P^{\bullet+}$ midpoint potential. [d] Value obtained from the extrapolation of eq 5 to $x = \infty$, with $E_L = 680$ meV. [e] Measured midpoint potential of the M202 heterodimer mutant of *Rb. sphaeroides* (*44*−*46*) where all of the positive charge resides on P_L. [f] Taken from ref *20*. [g] See Table 1 of this work. [h] As determined from FT Raman (*13*). [i] As determined from ENDOR (*47*) and Table 1.

$$\rho_L/\rho_M = x = \{\Delta\alpha/\beta_D + [(\Delta\alpha/\beta_D)^2 + 1]^{1/2}\}^2 \quad (2)$$

The $P^{o}/P^{\bullet+}$ redox midpoint potential, E_m, can be expressed as

$$E_m = E_L - \epsilon \quad (3)$$

and

$$\epsilon = (\Delta E - \Delta\alpha)/2 \quad (4)$$

where the energies E_L and ϵ are diagramatically shown in Figure 6. The $P^{o}/P^{\bullet+}$ redox midpoint potential can thus be rewritten as (*17*):

$$E_m = E_L - \{-[\beta_D(1- 2x + x^2)^{1/2}]/2x^{1/2} + [4\beta_D{}^2 + \beta_D{}^2(1 - 2x + x^2)/4x]^{1/2}\}/2 \quad (5)$$

This equation casts the $P^{o}/P^{\bullet+}$ redox midpoint potential, E_m, in terms of the ratio $x = \rho_L/\rho_m$ with the two constants E_L (HOMO energy of P_L) and β_D (the resonance integral).

The best fit for both the Raman and ENDOR data in Figure 5 was empirically determined by choosing values of E_L between 560 and 760 meV; these are values for the oxidation midpoint potentials of BChl *a* in various solvents (*43*) which should correspond to the HOMO energy of BChl in the respective solvents. Using $E_L = 560$ meV results in unacceptable fits despite what β_D value is used. In contrast, using $E_L = 760$ meV results in a better fit with a reasonable β_D value (i.e. ca, 150 meV or 1210 cm^{-1}); however, these β_D values result in a curve shape which does not accurately describe the data points. Good fits are obtained with $670 < E_L < 700$ meV and $250 > \beta_D > 200$ meV. Furthermore, the curve described by eq 5 extrapolates to a limiting value of E_L meV, since mathematically the ϵ term in eq 5 tends to be zero for large values of $x = \rho_L/\rho_M$ (which represents 100% localization of the positive charge on P_L). For the case of the M202 heterodimer RC mutant of *Rb. sphaeroides* where complete localization is on P_L, the P midpoint potential is 640−660 mV (*44*−*46*). Thus, the E_L value should be near 660 meV.

Using the above constraints, the best fit of eq 5 for both the Raman and ENDOR sets of data together is obtained with $E_L = 680$ meV and $\beta_D = 240$ meV (1940 cm^{-1}) with errors on these values estimated to be ± 40 meV (Table 3). These values apply to the wild-type dimer and compare well with $E_L = 700$ meV and $\beta_D = 220$ meV found by Artz et al. (*17*) based on the ENDOR data. Having found values for E_L and β_D using eq 5, the other energetic parameters, namely, E_M, ρ_L/ρ_M, $\Delta\alpha$, and ΔE may be found by substitution into eqs 1−4. Keeping $E_L = 680$ meV and $\beta_D = 240$ meV constant and substituting into eqs 1−4, we allowed the value of E_M to vary until the values for the midpoint potential E_m and ρ_L/ρ_M agreed with the experimentally determined values. Using this approach, we found that $E_M = 800$ meV yielded values of $E_m = 495$ meV and $\rho_L/\rho_M = 2.56$, in good agreement with the measured values as seen in the first row in Table 1, and consequently $\Delta\alpha = 120$ meV and $\Delta E = 494$ meV. We note that the values $E_m = 495$ meV and $\rho_L/\rho_M = 2.56$ do not strictly coincide with the values given by the line in Figure 5, since this line was obtained using eq 5 taking into consideration *all* of the wild-type and M160 mutant data points to arrive at E_L and β_D; E_M and ρ_L/ρ_M (as well as, consequently, $\Delta\alpha$, and ΔE) were obtained by taking into consideration *only* the experimentally determined E_m and ρ_L/ρ_M wild-type values, thus biasing the E_M parameter toward these latter observables for wild type.

The obtained energetic parameters of the P_L and P_M MO's, which reflect the electronic structure of the primary donor dimer, fall within the range of values of the redox potentials of isolated BChl *a* oxidation potentials in vitro (*43*), suggesting that the protein may not impart atypical redox properties to these BChl molecules as compared to many solvents.

Based on these results that E_M and E_L appear to be typical for BChl *a*, we have used the same asymmetric dimer model in order to see whether substituting a typical BPhe *a* oxidation potential would yield reasonable values for the oxidation midpoint potential of the M202 heterodimer mutant where the M-side primary donor constituent is a BPhe *a* and not a BChl *a* molecule. The oxidation potential of BPhe *a* in vitro is between ca. 1000 and 1100 mV. If we use the same parameters as we have found for the WT dimer, i.e., $E_L = 680$ meV, $\beta_D = 240$ meV, and simply substitute 1100 meV for E_M (instead of 800 meV) to represent the BPhe of the heterodimer, then we obtain an E_m value of 574 meV which is not in agreement with the $D^{o}/D^{\bullet+}$ redox midpoint potential of ca. 650 mV for the heterodimer. Indeed, one would need to substitute a value of ca. 2500 meV for E_M to obtain a $P^{o}/P^{\bullet+}$ redox midpoint potential of ca. 650 meV from the model. This rather high value of E_M, which is supposed to reflect the oxidation potential of BPhe *a*, seems unreasonably high. Thus, according to our model, it would appear that one of the parameters, i.e., E_L or β_D, for the heterodimer is different as compared to the WT.

Using a value of $\beta_D = 120$ meV, i.e., half of that found for the modeling of the WT dimer, along with $E_L = 680$ meV and $E_M = 1100$ meV, then we obtain a $D^{o}/D^{\bullet+}$ redox midpoint potential of 651 meV and $\rho_L/\rho_M = 50$, in agreement with the experimental values. Because the BChl and BPhe constituents of the heterodimer are not strictly the same molecule, one could expect a change in the coupling between them, although, arguably, changing β_D by a factor of 2 may

seem unreasonable. Alternatively, a +100 meV change in the value of E_L in the heterodimer would also yield a midpoint potential in agreement with experiment; however, the predicted ρ_L/ρ_M value is significantly lower. For E_L = 780 meV and β_D = 240 meV, the calculated $D^{o}/D^{\bullet+}$ midpoint potential is 654 meV and $\rho_L/\rho_M = 9$.

X-ray crystallographic data (*7*) suggest that there are no drastic secondary changes in the protein environment of the heterodimer primary donor (*29*) apart from the His M202 to Leu mutation and incorporation of a BPhe molecule instead of BChl for the P_M constituent. Thus, one could expect that the E_L and β_D parameters should not sizeably change. Fixing one of these parameters requires large changes in the other, as described above. By modestly changing both the E_L and β_D parameters by 50 meV (i.e., E_L + 50 meV = 730 meV, β_D − 50 meV = 190 meV), we obtain a heterodimer $D^{o}/D^{\bullet+}$ midpoint potential of 652 meV and $\rho_L/\rho_M = 17$. Thus, according to our simple model, the higher oxidation potential of the heterodimer can be understood in terms not only of the higher oxidation potential of the BPhe molecule (as compared to BChl) but also in a modest decrease in the resonance interaction between the two different chromophores of the heterodimer compared to the homodimer case of WT as well as a modest increase in the HOMO energy of the P_L constituent.

SUMMARY

There is a general correlation between the strength and number of H-bonds to the conjugated C_2 and C_9 carbonyl groups of P and the rise in $P^{o}/P^{\bullet+}$ redox midpoint potential. This correlation appears to be linear within the regime of the strength of the H-bonds we have studied, but the exact description of the correlation appears to be dependent on the chemical nature of the H-bond-donating residue. Histidine residues are the most effective in raising the midpoint potential for a given H-bond strength. These, single, H-bonds formed or ruptured have estimated enthalpies varying between 90 and 200 meV and can raise the midpoint potential by 60−125 mV.

The effect of the H-bonds in raising the $P^{o}/P^{\bullet+}$ redox midpoint potential can be explained by the stabilization (lowering in energy) of the P_L and P_M HOMOs, which has a predictable effect on the modulation of the percent localization of the positive charge over $P^{\bullet+}$. Modeling the primary donor dimer MOs using a simple asymmetric dimer model of Hückel-type MOs suggests that the HOMO energies of the constituent P_L and P_M monomers are very similar to those of BChl *a* in typical solvents, suggesting that the protein does not impart atypical redox properties to P_L and P_M except, perhaps, to fix them in position to form a dimer.

Factors other than H-bonding are certainly at work. For point mutations not resulting in H-bonding to the primary donor, the redox potential can vary up to 60 mV. These factors are presumably electrostatic in nature and need further work to elucidate.

ACKNOWLEDGMENT

We thank X. Nguyen for assistance with the construction of the strains and the isolation of the reaction centers, and M. Roy for contributions with the measurement of the redox midpoint potentials. A.I. acknowledges Marc Lutz (CEA/Saclay) for his interest in this work.

REFERENCES

1. Parson, W. W. (1991) in *Chlorophylls* (Scheer, H., Ed.) pp 1153−1180, CRC Press, Boca Raton.
2. Kirmaier, C., and Holten, D. (1993) in *The Photosynthetic Reaction Center* (Deisenhofer, J., and Norris, J. R., Eds.) Vol. II, pp 49−70, Academic Press, San Diego.
3. Woodbury, N. W., and Allen, J. P. (1995) in *Anoxygenic Photosynthetic Bacteria* (Blankenship, R. E., Madigan, M. T., and Bauer, C. E., Eds.) pp 527−557, Kluwer, Dordrecht, The Netherlands.
4. Deisenhofer, J., Epp, O., Miki, K., Huber, R., and Michel, H. (1985) *Nature 318*, 618−624.
5. Allen, J. P., Feher, G., Yeates, T. O., Komiya, H., and Rees, D. C. (1987) *Proc. Natl. Acad. Sci. U.S.A. 84*, 5730−5734.
6. El-Kabbani, O., Chang, C.-H., Tiede, D., Norris, J., and Schiffer, M. (1991) *Biochemistry 30*, 5361−5369.
7. Chirino, A. J., Lous, E. J., Huber, M., Allen, J. P., Schenck, C. C., Paddock, M. L., Feher, G., and Rees, D. C. (1994) *Biochemistry 33*, 4584−4593.
8. Ermler, U., Fritzsch, G., Buchanan, S. K., and Michel, H. (1994) *Structure 2*, 925−936.
9. Deisenhofer, J., Epp, O., Sinning, I., and Michel, H. (1995) *J. Mol. Biol. 246*, 429−457.
10. Arnoux, B., and Reiss-Husson, F. (1996) *Eur. Biophys. J. 24*, 233−242.
11. Allen, J. P., and Williams, J. C. (1995) *J. Bioenerg. Biomembr. 27*, 275−283.
12. Lin, X., Murchison, H. A., Nagarajan, V., Parson, W. W., Williams, J. C., and Allen, J. P. (1994) *Proc. Natl. Acad. Sci. U.S.A. 91*, 10265−10269.
13. Mattioli, T. A., Lin, X., Allen, J. P., and Williams, J. C. (1995) *Biochemistry 34*, 6142−6152.
14. Mattioli, T. A., Williams, J. C., Allen J. P., and Robert, B. (1994) *Biochemistry 33*, 1636−1643.
15. Wachtveitl, J., Farchaus, J. W., Das, R., Lutz, M., Robert, B., and Mattioli, T. A. (1993a) *Biochemistry 32*, 12875−12886.
16. Nabedryk, E., Allen, J. P., Taguchi, A. K. W., Williams, J. C., Woodbury, N. W., and Breton, J. (1993) *Biochemistry 32*, 13879−13885.
17. Artz, K., Williams, J. C., Allen, J. P., Lendzian, F., Rautter, J., and Lubitz, W. (1997) *Proc. Natl. Acad. Sci. U.S.A. 94*, 13582−13587.
18. Plato, M., Lendzian, F., Lubitz, W., and Möbius, K. (1992) in *The Photosynthetic Bacterial Reaction Center II* (Breton, J., and Verméglio, A., Eds.) pp 109−118, Plenum Press, New York.
19. Parson, W. W., Nabedryk, E., and Breton, J. (1992) in *The Photosynthetic Bacterial Reaction Center II* (Breton, J., and Verméglio, A., Eds.) pp 79−88, Plenum Press, New York.
20. Breton, J., Nabedryk, E., and Parson, W. W. (1992) *Biochemistry 31*, 7503−7510.
21. Williams, J. C., Alden, R. G., Murchinson, H. A., Peloquin, J. M., Woodbury, N. W., and Allen, J. P. (1992) *Biochemistry 31*, 11029−11037.
22. Murchison, H. A., Alden, R. G., Allen, J. P., Peloquin, J. M., Taguchi, A. K. W., Woodbury, N. W., and Williams, J. C. (1993) *Biochemistry 32*, 3498−3505.
23. Lin, X., Williams, J. C., Allen, J. P., and Mathis, P. (1994b) *Biochemistry 33*, 13517−13523.
24. Paddock, M. L., Rogney, S. H., Feher, G., and Okamura, M. Y. (1989) *Proc. Natl. Acad. Sci. U.S.A. 86*, 6602−6606.
25. Mattioli, T. A., Hoffmann, A., Robert, B., Schrader, B., and Lutz, M. (1991) *Biochemistry 30*, 4648−4654.
26. Ivancich, A., Feick, R., Ertlmaier, A., and Mattioli, T. A. (1996a) *Biochemistry 35*, 6126−6135.
27. Ivancich, A., Kobayashi, M., Drepper, F., Fathir, I., Saito, T., Nozawa, T., and Mattioli, T. A. (1996b) *Biochemistry 35*, 10529−10538.

28. Mattioli, T. A., Hoffmann, A., Sockalingum, D., Schrader, B., Robert, B., and Lutz, M. (1993) *Spectrochim. Acta 49A*, 785−799.
29. Albouy, D., Kuhn, M., Williams, J. C., Allen, J. P., Lubitz, W., and Mattioli, T. A. (1997) *Biochim. Biophys. Acta 1321*, 137−148.
30. Cotton, T. M., Parks, K. D., and Van Duyne, R. P. (1980) *J. Am. Chem. Soc. 102*, 6399−6407.
31. Mäntele, W. G., Wollenwebber, A. M., Nabedryk, E., and Breton, J. (1988) *Proc. Natl. Acad. Sci. U.S.A. 85*, 8468−8472.
32. Heald, R. L., and Cotton, T. M. (1990) *J. Phys. Chem. 94*, 3968−3975.
33. Diers, J. R., and Bocian, D. F. (1994) *J. Phys. Chem. 98*, 12884−12892.
34. Nagarajan, V., Parson, W. W., Davis, D., and Schenck, C. C. (1993) *Biochemistry 32*, 12324−12336.
35. Wachtveitl, J., Farchaus, J. W., Mathis, P., and Oesterhelt, D. (1993b) *Biochemistry 32*, 10894−10904.
36. Parson, W. W., and Warshel, A. (1987) *J. Am. Chem. Soc. 109*, 6152−6163.
37. Ivancich, A., Mattioli, T. A., Artz, K., Wang, S., Allen, J. P., and Williams, J. C. (1997) *Biochemistry 36*, 3027−3036.
38. Grimmett, M. R. (1970) *Adv. Heterocycl. Chem*. 12, 103−183.
39. Fajer, J., Barkigia, K. M., Smith, K. M., Zhong, E., Gudowska-Novak, E., and Newton, M. D. (1990) in *Reaction Centers of Photosynthetic Bacteria: Structure and Dynamics* (Michel-Beyerle, M. E., Ed.) pp 367−376, Springer-Verlag, Berlin.
40. Haley, L. V., and Koningstein, J. A. (1983) *Can. J. Chem. 61*, 14−20.
41. Reimers, J. R., and Hush, N. S. (1996) *Chem. Phys. 208*, 177−193.
42. Gasyna, Z., and Schatz, P. N. (1996) *J. Phys. Chem. 100*, 1445−1448.
43. Watanabe, T., and Kobayashi, M. (1991) in *Chlorophylls* (Scheer, H., Ed.) pp 287−315, CRC Press, Boca Raton, FL.
44. Davis, D., Dong, A., Caughey, W. S., and Schenck, C. C. (1992) *Biophys. J. 61*, A153.
45. Laporte, L. L., Palaniappan, V., Davis, D. G., Kirmaier, C., Schenck, C. C., Holten, D., and Bocian, D. F. (1996) *J. Phys. Chem. 100*, 17696−17707.
46. Allen, J. P., Artz, K., Lin, X., Williams, J. C., Ivancich, A., Albouy, D., Mattioli, T. A., Fetsch, A., Kuhn, M., and Lubitz, W. (1996) *Biochemistry 35*, 6612−6619.
47. Lendzian, F., Huber, M., Isaacson, R. A., Endeward, B., Plato, M., Bonigk, B., Möbius, K., Lubitz, W., and Feher, G. (1993) *Biochim. Biophys. Acta 1183*, 139−160.

BI9806908